Article

克级自下而上闪蒸石墨烯合成

Gram-scale bottom-up flash graphene synthesis

https://doi.org/10.1038/s41586-020-1938-0

Received: 28 May 2019

Accepted: 22 October 2019

Published online: 27 January 2020

Duy X. Luong[1,2], Ksenia V. Bets[3], Wala Ali Algozeeb[2], Michael G. Stanford[2], Carter Kittrell[2], Weiyin Chen[2], Rodrigo V. Salvatierra[2], Muqing Ren[2], Emily A. McHugh[2], Paul A. Advincula[2], Zhe Wang[2], Mahesh Bhatt[4], Hua Guo[3], Vladimir Mancevski[2], Rouzbeh Shahsavari[4,5]*, Boris I. Yakobson[2,3,6]* & James M. Tour[2,3,6]*

大多数大块石墨烯是通过自上而下的方法生产的，即剥离石墨，这通常需要大量的溶剂进行高能混合、剪切、超声或电化学处理。
Most bulk-scale graphene is produced by a top-down approach, exfoliating graphite, which often requires large amounts of solvent with high-energy mixing, shearing, sonication or electrochemical treatment[1–3]. 虽然石墨化学氧化为氧化石墨烯会促进剥离，但它需要苛刻的氧化剂，并且在随后的还原步骤后，石墨烯会留下有缺陷的穿孔结构。如果通过化学气相沉积或先进的合成有机方法进行，高质量石墨烯的自下而上合成通常仅限于超少量，或者如果在大量溶液中进行，则生成满是缺陷的结构。
Although chemical oxidation of graphite to graphene oxide promotes exfoliation, it requires harsh oxidants and leaves the graphene with a defective perforated structure after the subsequent reduction step[3,4]. Bottom-up synthesis of high-quality graphene is often restricted to ultrasmall amounts if performed by chemical vapour deposition or advanced synthetic organic methods, or it provides a defect-ridden structure if carried out in bulk solution[4–6]. 在这里，我们表明，对廉价碳源（如煤、石油焦、生物炭、炭黑、废弃食品、橡胶轮胎和混合塑料废物）进行快速焦耳加热，可以在不到1秒的时间内获得克级石墨烯。
Here we show that flash Joule heating of inexpensive carbon sources—such as coal, petroleum coke, biochar, carbon black, discarded food, rubber tyres and mixed plastic waste—can afford gram-scale quantities of graphene in less than one second. 该产品因其生产工艺而命名为闪蒸石墨烯（FG），在堆叠的石墨烯层之间显示出涡轮层状排列（即微有序）。
The product, named flash graphene (FG) after the process used to produce it, shows turbostratic arrangement (that is, little order) between the stacked graphene layers. FG合成不使用熔炉，也不使用溶剂或反应性气体。产量取决于碳源的碳含量；当使用炭黑、无烟煤或煅烧焦炭等高碳源时，产量可在80%至90%之间，碳纯度大于99%。
FG synthesis uses no furnace and no solvents or reactive gases. Yields depend on the carbon content of the source; when using a high-carbon source, such as carbon black, anthracitic coal or calcined coke, yields can range from 80 to 90 per cent with carbon purity greater than 99 per cent. 无需净化步骤。拉曼光谱分析显示FG具有低强度或缺失的D带，表明FG是迄今为止报道的石墨烯最低缺陷浓度之一，并证实了FG是涡轮状堆叠的，这与涡轮层叠石墨明显不同。
No purification steps are necessary. Raman spectroscopy analysis shows a low-intensity or absent D band for FG, indicating that FG has among the lowest defect concentrations reported so far for graphene, and confirms the turbostratic stacking of FG, which is clearly distinguished from turbostratic graphite. FG层的无序取向有利于其在复合材料形成过程中混合后快速剥离。
The disordered orientation of FG layers facilitates its rapid exfoliation upon mixing during composite formation. FG合成的电能成本仅为约7.2千焦耳/克，这可能使FG适合用于塑料、金属、胶合板、混凝土和其他建筑材料的大块复合材料。
The electric energy cost for FG synthesis is only about 7.2 kilojoules per gram, which could render FG suitable for use in bulk composites of plastic, metals, plywood, concrete and other building materials.

在快速焦耳加热（FJH）过程中，非晶导电碳粉在两个电极之间的石英管或陶瓷管内被轻微压缩（图1a，补充图1）。
In the flash Joule heating (FJH) process, amorphous conductive carbon powder is lightly compressed inside a quartz or ceramic tube between two electrodes (Fig. 1a, Supplementary Fig. 1). 该系统可以在大气压力下，或在轻度真空（约10毫米汞柱）下，以便于排气。
The system can be at atmospheric pressure, or under a mild vacuum (~10 mm Hg) to facilitate outgassing. 电极可以是铜、石墨或任何导电耐火材料，它们松散地安装在石英管中，以允许FJH排气。
The electrodes can be copper, graphite or any conductive refractory material, and they fit loosely into the quartz tube to permit outgassing upon FJH. 电容器组的高压放电使碳源在不到100 ms的时间内达到3000 K以上的温度，有效地将非晶态碳转化为涡轮层状FG。
High-voltage electric discharge from a capacitor bank brings the carbon source to temperatures higher than 3,000 K in less than 100 ms, effectively converting the amorphous carbon into turbostratic FG. 在高分辨率透射电子显微镜（HR-TEM）分析中（图1b，c），FG的取向错配层显示出预期的莫尔条纹，而从废咖啡渣中提取的FG也显示出六方单层石墨烯（图1d）。
In high-resolution transmission electron microscopy (HR-TEM) analysis (Fig. 1b, c), the misoriented layers of FG exhibit the expected Moiré patterns, whereas FG derived from spent coffee grounds also shows hexagonal single-layer graphene (Fig. 1d). 高质量的石墨烯可以通过拉曼光谱快速表征。炭黑的FG（CB-FG）有一个强的2D峰。
High-quality graphene can be quickly identified by Raman spectroscopy[7–10]. FG from carbon black (CB-FG) has an intense 2D peak. As seen in the Raman mapping of CB-FG in Fig. 1e, the intensity of the 2D band relative to the G band ($I_{2D/G}$) is greater than 10 in many locations. 从图1e中CB-FG的拉曼映射中可以看出，2D带相对于G带（I2D/G）的强度在许多位点大于10。D带的极低强度表明这些FG产品的缺陷浓度较低，这有助于2D带的放大。
The extremely low intensity of the D band indicates the low defect concentration of these FG products, which contributes to the amplification of the 2D band. Thus, the unusually high $I_{2D/G}$ = 17 (Fig. 1e) of CB-FG is the highest value reported so far for any form of graphene, and is probably an outcome of the extreme temperature reached in the flash process, which outgasses non-carbon elements from the system. 因此，CB-FG的异常高I2D/G=17（图1e）是迄今为止任何形式石墨烯的最高报道值，可能是闪蒸过程中达到的极端温度的结果，该过程会将非碳元素从体系中排出。
Additionally, the two peaks TS_1 and TS_2 at ~1,886 cm^{-1} and ~2,031 cm^{-1}, respectively, confirm the turbostratic nature of FG (Supplementary Figs. 2, 3), which is discussed extensively in Supplementary Information and Supplementary Table 1[11,12]. 此外，分别位于约1886 cm-1和约2031 cm-1处的两个峰值TS1和TS2证实了FG的涡轮层状性质（补充图2,3）。补充信息和补充表对此进行了广泛讨论。
The X-ray diffraction (XRD) pattern of FG shows a well defined (002) peak indicating successful graphitization of the amorphous carbon. FG的X射线衍射（XRD）图显示了一个明确的(002)峰，表明非晶碳成功石墨化。
The (002) peak of FG occurs at diffraction angle $2\theta = 26.1°$, FG的(002)峰值出现在衍射角2θ=26.1°时，对应于层间距Ic=3.45。

[1]Applied Physics Program, Rice University, Houston, TX, USA. [2]Department of Chemistry, Rice University, Houston, TX, USA. [3]Department of Materials Science and NanoEngineering, Rice University, Houston, TX, USA. [4]C-Crete Technologies, Stafford, TX, USA. [5]Department of Civil and Environmental Engineering, Rice University, Houston, TX, USA. [6]Smalley-Curl Institute and the NanoCarbon Center, Rice University, Houston, TX, USA. *e-mail: rouzbeh@ccretetech.com; biy@rice.edu; tour@rice.edu

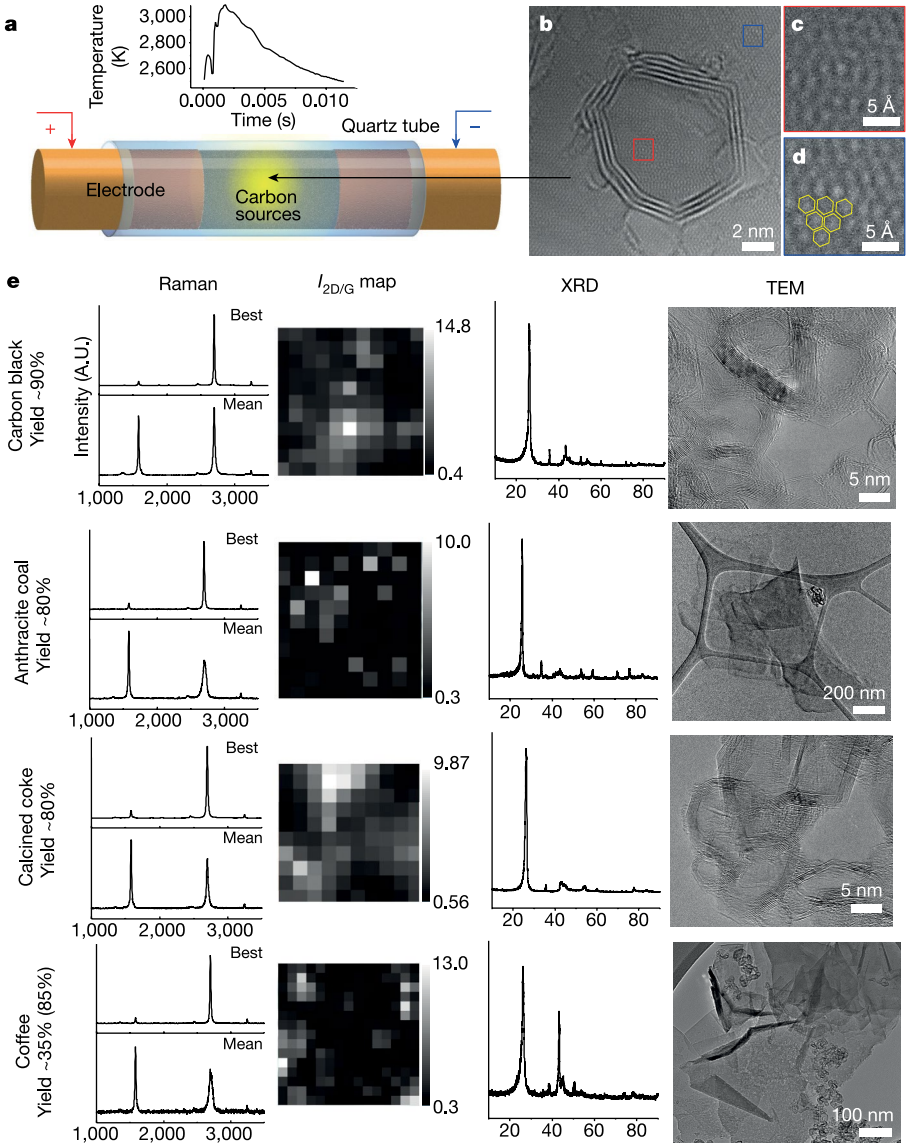

图1. 从各种碳源合成的FG。 a. FJH过程示意图

Fig. 1 | FG synthesized from various carbon sources. a, Schematic of the FJH 以及闪蒸期间升温与时间的关系图(插图)。
process, and plot of the temperature rise versus time during flashing (inset). b-d, 咖啡制备的单层FG上面CB-FG的HR-TEM图像。
b–d, HR-TEM image of CB-FG on top of a single layer of coffee-derived FG. e. 表征结果，包括来自不同碳源的FG的拉曼光谱(显示最佳和平均获得的谱)、XRD光谱和TEM图像。
e, Characterization results, including Raman spectra (showing the best and the mean obtained spectra), XRD spectra and TEM images for FG derived from 咖啡衍生FG由使用过的咖啡渣制成；大石墨烯片中较小的石墨烯颗粒
various carbon sources. The coffee-derived FG is made from used coffee grounds; the smaller graphene particles within large graphene sheets come 来自炭黑导电添加剂。 使用50倍放大率，拉曼映射中的每个像素为4 μm2。
from the carbon black conductive additive. Each pixel in the Raman mapping is 所有拉曼样品均由粉末状产物经FJH后制备；拉曼分析之前，样品
$4\ \mu m^2$ using a 50× magnification. All Raman samples were prepared from the 未接触溶剂。
powdered product after FJH; the samples were not exposed to the solvent 咖啡含碳量约为40%，因此，根据起始含碳量，产率约为85%。
before Raman analysis. Coffee is about 40% carbon, so the yield based on the 平均拉曼光谱的样本量为10。
starting carbon content is ~85%. The sample size for the mean Raman spectrum is 10.

该间距大于典型
which corresponds to an interlayer spacing of I_c = 3.45 Å. This spacing Bernal(AB堆积)石墨中的间距3.37，表明FG具有膨胀和涡轮层状结构。
is larger than that in a typical Bernal (AB-stacked) graphite, 3.37 Å, indicating the expanded and turbostratic structure of FG. The (002) 可以看到(002)峰不对称，尾部呈小角度，这进一步证明了FG的涡轮层性质。
peak was found to be unsymmetric, with a tail at small angles, which 闪蒸过程足够快，可以防止
further suggests the turbostratic nature of FG[13]. The flash process AB堆叠。 根据Brunauer-Emmett-Teller分析测定，
is fast enough to prevent AB stacking. CB-FG has a surface area of CB-FG的表面积约为295m2/g，孔径<9nm(补充图4)。
~295 $m^2\ g^{-1}$ with pore size <9 nm, as measured by Brunauer–Emmett– 煅烧石油焦(CPC)也可以很好地转化
Teller analysis (Supplementary Fig. 4). Calcined petroleum coke 为CPC-FG(图1e，补充表2)，CPC-FG具有与CB-FG相似的纳米结构。
(CPC) also works well for conversion to CPC-FG (Fig. 1e, Supplementary Table 2) which has a similar nanostructure to that of CB-FG. CPC与炭黑一起被列为难石墨化碳源(补充表3)。
Together with carbon black, CPC is listed as a non-graphitized carbon CB-FG和CPC-FG的平均尺寸分别为约13nm和
source (Supplementary Table 3)[14]. The average size of CB-FG and CPC- 约17nm(补充图5,6)。
FG is ~13 nm and ~17 nm, respectively (Supplementary Figs. 5, 6). The FJH方法的产量高达80%-90%，来自炭黑、煅烧焦炭或无烟煤等高碳源，以及
yield of the FJH process is as high as 80% to 90% from high-carbon sources such as carbon black, calcine coke or anthracite coal, and

转换所需的电能约为7.2 kJ/g(补充信息)。
the electric energy needed for their conversion is ~7.2 kJ g^{-1} (Supplementary Information). 在咖啡渣的情况下，使用过的咖啡渣与5 wt%的炭黑混合以增加其导电性。
In the case of coffee grounds, the used grounds were mixed with 或者，我们可以使用之前运行的2-5 wt% FG作为导电添加剂。
5 wt% carbon black to increase its conductivity—alternatively, we could use 2–5 wt% FG from a previous run as the conductive additive. Coffee 咖啡渣主要是碳水化合物，含碳量约为40%。 因此，石
grounds, being predominantly carbohydrate, are ~40% carbon. Hence, 墨烯的产率约为35%(图1e)，咖啡碳含量转化为石墨烯的转化率约为85%，而杂原子在这些反应温
the yield of graphene of ~35% (Fig. 1e) would be ~85% conversion of the 度(>3000 K)下开华。
coffee carbon content into graphene, whereas the heteroatoms sublime 无烟煤具有足够的导电性，可用
out at these reaction temperatures (>3,000 K). Anthracite can be suf- 于FJH反应器，但添加5 wt%的炭黑可获得更好的结果。
ficiently conductive to be used in the FJH reactor, but better results were 尽管不管原料是什么，都会生产出黑色FG
obtained by adding 5 wt% carbon black. Although a black FG powder 粉末，但从易石墨化碳中提取的FG，如从废咖啡渣(C-FG)和无烟煤(a-FG)中提取的FG(有关
is produced regardless of the starting material, FG from graphitizing 易石墨化和难石墨化碳的定义，请参见补充信息；另请参见补充表3)具有以下特点：
carbons—such as from used coffee grounds (C-FG) and anthracite coal (A-FG) (see Supplementary Information for definitions of graphitizing and non-graphitizing carbons; see also Supplementary Table 3)—has

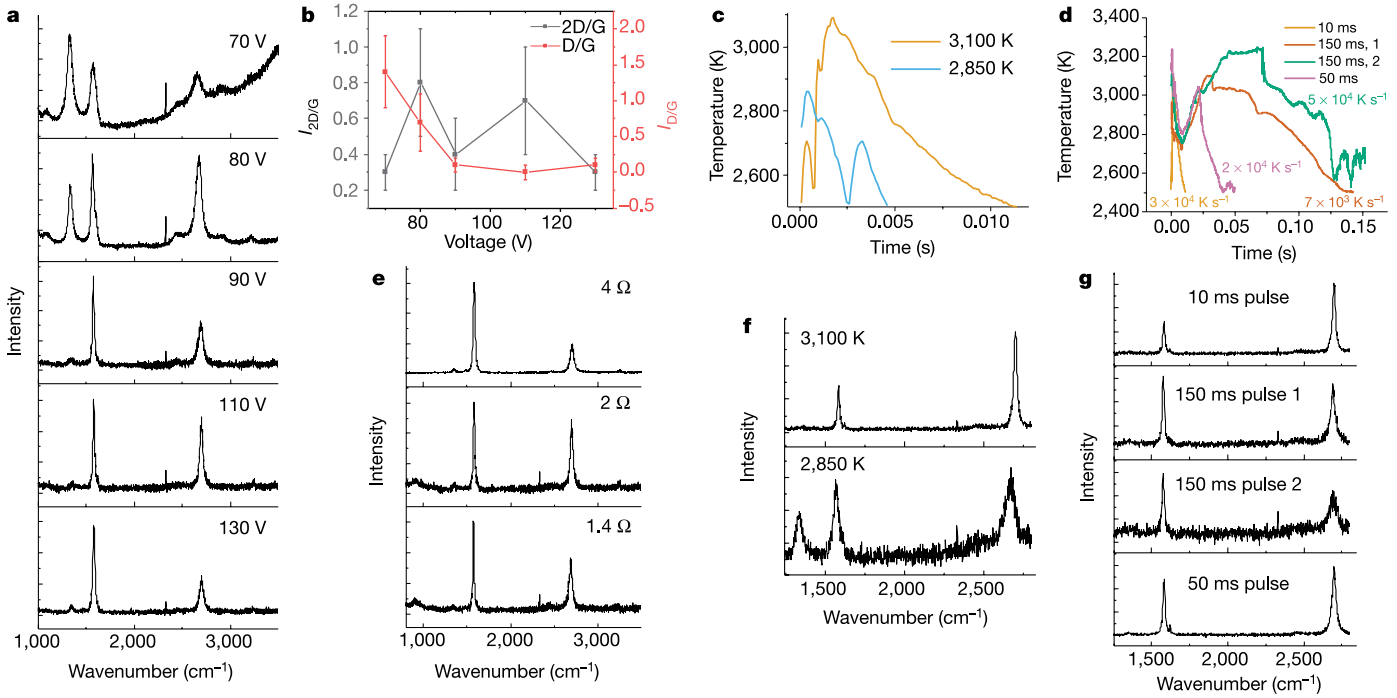

图2. FJH临界参数。 a. CB-FG的拉曼光谱随闪蒸电压的增加(从上到下)。 b. 不同闪蒸电压下CB-FG的I2D/G和ID/G比。 条形代表1个标准偏差。 c. CB-FG在不同温度下反应的时间-温度图。 温度由闪蒸电压调节。 d. CB-FG在不同闪蒸时间下反应的时间-温度图。 闪蒸时间由电极之间的样品压缩来调节，它影响样品的电导率。 图中的数字表示冷却速率。 e. 拉曼光谱 较高的压缩可降低样品的电阻。 f. CB-FG样品的拉曼光谱如c所示。 g. CB-FG样品的拉曼光谱如d所示。 150 ms脉冲1和2的持续时间相似，但冷却速率不同，如d所示。 图中的所有拉曼光谱都是在低倍率(5×)下获得的，从10个谱平均得到样品的平均光谱。

Fig. 2 | FJH critical parameters. a, Raman spectra of CB-FG with increasing flashing voltage (top to bottom). **b**, $I_{2D/G}$ and $I_{D/G}$ ratios of CB-FG at different flashing voltages. The bars represent 1 s.d. (n = 10). **c**, Time–temperature graph of CB-FG reacted at different temperatures. The temperature is regulated by the flashing voltage. **d**, Time–temperature graph of CB-FG reacted at different flashing durations. The flashing duration is regulated by the sample compression between the electrodes, which affects the sample conductivity. The numbers within the plot represent cooling rates. **e**, Raman spectra of CB-FG at different compression ratios. Higher compression provides lower resistance to the sample. **f**, Raman spectra of the CB-FG samples shown in **c**. **g**, Raman spectra of the CB-FG samples shown in **d**. The 150-ms pulses 1 and 2 have similar duration but different cooling rates, as shown in **d**. All Raman spectra in the figure were taken at low magnification (5×) to obtain a mean spectrum of the sample from 10 spectra.

CB-FG的不同形态。 易石墨化碳产生较大的石墨烯片(补充图7)。 C-FG的XRD分析显示，除了26.0°处的主峰(002)外，2θ=42.5°处的尖峰(100)与面内原子间距有关(图1e)。 (100)峰窄的半高宽表明，相对于由一些其他起始材料形成的FG，平面内片层尺寸更大。 HR-TEM显示A-FG和C-FG中的折叠石墨烯片(图1e)，平均尺寸分别为0.5 μm和1.2 μm(补充图7)，类似于通过石墨剥离获得的石墨烯片的尺寸。 这些样品上的选区电子衍射测量显示单层石墨烯和两轮层石墨烯(补充图8–10)。

different morphologies from CB-FG. Graphitizing carbons produce larger graphene sheets (Supplementary Fig. 7). XRD analysis of C-FG shows, in addition to the dominant (002) peak at 26.0°, a sharp (100) peak at $2\theta = 42.5°$, which is associated with the in-plane interatomic spacing (Fig. 1e). The narrow full width at half-maximum of the (100) peak suggests larger in-plane sheet sizes relative to FG formed from some of the other starting materials. HR-TEM reveals folded graphene sheets in A-FG and C-FG (Fig. 1e) with an average size of 0.5 μm and 1.2 μm (Supplementary Fig. 7), similar to the size of graphene sheet obtained by exfoliation of graphite[3,15,16]. Selected-area electron diffraction measurements on these samples show both monolayer and turbostratic graphene (Supplementary Figs. 8–10).

可以使用其他丰富、可再生或废物来源的碳，如木炭、生物炭、腐殖酸、角蛋白(人发)、木质素、蔗糖、淀粉、松树皮、橄榄油烟尘、卷心菜、椰子、开心果壳、土豆皮、橡胶轮胎和混合塑料(补充图11，补充表4)，包括聚对苯二甲酸乙二醇酯(PET或PETE)，高密度或低密度聚乙烯、聚氯乙烯、聚丙烯和聚丙烯腈。 当合成的聚合物转化为FG时，非碳原子升华为小分子，从而生成含碳量非常高的产物，如图所示。

Other carbons that are abundant, renewable or waste-sourced can be used, such as charcoal, biochar, humic acid, keratin (human hair), lignin, sucrose, starch, pine bark, olive oil soot, cabbage, coconut, pistachio shells, potato skins, rubber tyres and mixed plastic (Supplementary Fig. 11, Supplementary Table 4), including polyethylene terephthalate (PET or PETE), high- or low-density polyethylene, polyvinyl chloride, polypropylene and polyacrylonitrile. When converting synthetic polymers into FG, the non-carbon atoms sublime out as small molecules, leading to a very-high-carbon-content product, as shown here. However, polymer and rubber depolymerization can also ensue to afford oligomers that sublime before conversion; therefore, it is more economical to use a pyrolysis product where the volatiles are first industrially removed for fuel sources[17] and the residual carbon is converted into FG. This was demonstrated here with rubber-tyre-derived carbon black (Supplementary Fig. 11, Supplementary Tables 2, 4). None of these FG processes was optimized. Optimization was performed only on CB-FG, as described below. The FJH process can provide a facile route to convert these waste products into FG, a potential high-value building-composite additive[18–21].

石墨烯I2D/G通过调整电极之间的样品压缩(影响样品电导率)、电容器电压和开关持续时间来优化，以控制闪蒸的温度和持续时间(图2a–g)。 增加电压将提高工艺温度。 通过拟合600–1100 nm发射中的黑体辐射光谱来估计温度(补充图12)。 我们通过改变FG合成过程中的时间和温度，利用低倍率拉曼光谱(见方法)研究了CB-FG的质量。 在<90 V和<3000 K时，FG具有高D峰值，表明存在缺陷结构(图2a–c，f)。 通过增加电压输出，可在3100 K下形成CB-FG，其缺陷数量较少，拉曼光谱中几乎没有D带。 因此，3000 K是制备具有较大I2D/G值的高质量石墨烯的临界温度。

The graphene $I_{2D/G}$ is optimized by adjusting the sample compression between the electrodes (which affects sample conductivity), the capacitor voltage and the switching duration to control the temperature and duration of the flash (Fig. 2a–g). Increasing the voltage will increase the temperature of the process. The temperature is estimated by fitting the black-body radiation spectrum in the 600–1,100 nm emission (Supplementary Fig. 12). We investigated the quality of CB-FG using Raman spectroscopy at low magnification (see Methods) by varying the time and temperature in the FG synthesis process. At <90 V and <3,000 K, FG has a high D peak, indicating a defective structure (Fig. 2a–c, f). By increasing the voltage output, CB-FG is formed at 3,100 K, which has a low number of defects and almost no D band in the Raman spectrum. Therefore, 3,000 K is a critical temperature for producing higher-quality graphene with a larger $I_{2D/G}$ value.

通过增加两个电极之间样品的压缩，碳源的电导率增加，从而缩短放电时间(图2d，e，g)。 在将两次实验之间的闪蒸温度保持在3100 K左右的情况下，10 ms的短闪蒸时间会产生较高的2D带，而50–150 ms的闪蒸时间会产生较低2D带的产物(图2g)。 这表明，如果时间更长，石墨烯薄片会堆叠、定向并形成更多层，从而降低最终FG的2D带。 低冷却速率会增加闪蒸持续时间并降低2D带。 因此，为了获得高的I2D/G，选择了一根细石英管来加速辐射冷却速率。 有趣的是，尽管内部温度超过3000 K，但石英管的外壁在闪蒸过程后仅达到可触摸的温度(<60 °C)。 大部分热量以黑体辐射形式放出。

By increasing the compression on the sample between the two electrodes, the conductivity of the carbon source increases, thus decreasing the discharge time (Fig. 2d, e, g). While maintaining the flash temperature between experimental runs at ~3,100 K, a short flash duration of 10 ms results in a higher 2D band, whereas a flash of 50–150 ms results in a lower 2D band product (Fig. 2g). This indicates that, given more time, the graphene flakes stack, orient and form more layers, lowering the 2D band of the resulting FG. A low cooling rate increases the flash duration and decreases the 2D band[22]. Therefore, to obtain a high $I_{2D/G}$, a thin quartz tube is chosen to accelerate the radiative cooling rate. Interestingly, although the internal temperatures exceed 3,000 K, the external walls of the quartz tubes are only warm to the touch (<60 °C) after the flash process. Most of the heat exits as black-body radiation.

X射线光电子能谱分析表明，FG中除碳以外的元素大量减少，sp2碳键含量增加(补充图13,14)。

X-ray photoelectron spectroscopy analysis shows a considerable reduction of elements other than carbon in FG and increases in the sp^2 carbon bond content (Supplementary Figs. 13, 14). Carbon has a

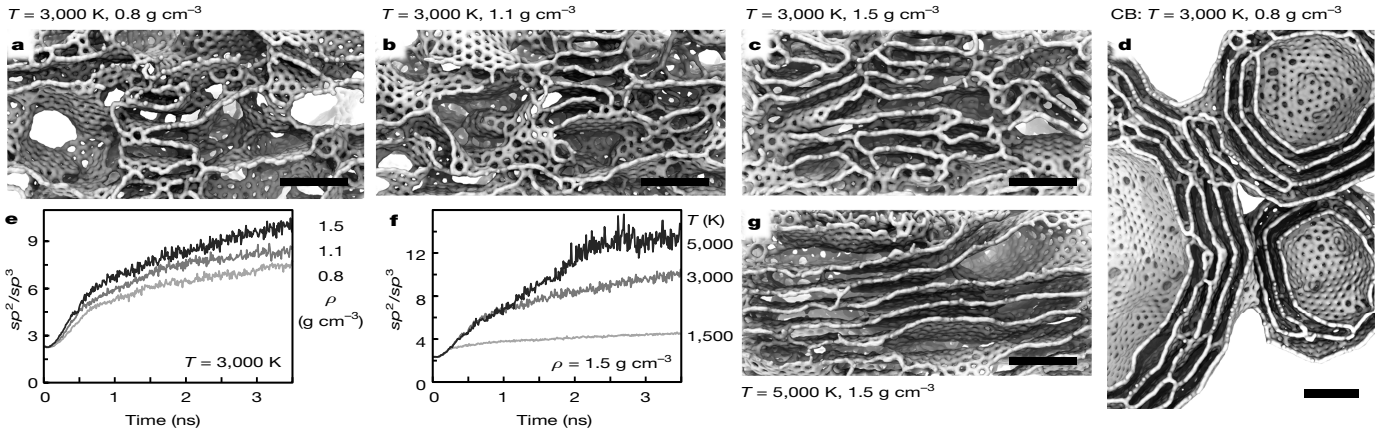

图3. 分子动力学模拟。具有各种

Fig. 3 | Molecular dynamics simulations. Structures with various

使用Nos é -Hoover恒温器，在给定温度范围(1500至5000 K)下保持5×10 -9 s的特性(如微孔隙、错位

characteristics (such as micro-porosity, misalignment and size of graphitic

和石墨畴的大小)。

domains) kept at a given temperature range (1,500 to 5,000 K) for up to 5×10^{-9} s

a-c，密度为0.8 g/cm3(a；海绵状结构)、1.1 g/cm3

with a Nosé–Hoover thermostat. **a**–**c**, Sample structures for carbon materials of

(b)和1.5 g/cm3(c；高度石墨化)的碳材料在3000 K. d. 退火后的样品结构，炭黑

density 0.8 g cm^{-3} (**a**; sponge-like structure), 1.1 g cm^{-3} (**b**), and 1.5 g cm^{-3} (**c**; high

degree of graphitization) after annealing at 3,000 K. **d**, Carbon black with

在3600 K下长时间(5×10 -9 s)退火后，密度为0.8 g/cm3，宏观孔隙率大；多边形条纹很明显。

density 0.8 g cm^{-3} and large macro-porosity, after prolonged (5×10^{-9} s)

e,f，不同密度材料(e)

annealing at 3,600 K; polygonal fringes are apparent. **e**–**f**, Change of the

和不同温度下退火时材料结构成分的变化T(f)。

structural composition of materials during annealing for materials of different

g, 5000 K退火后密

densities ρ (**e**) and for annealing at different temperatures T (**f**). **g**, Structure of

度为1.5 g/cm3的材料结构；初始结构与c所示相同。

material with density 1.5 g cm^{-3} after annealing at 5,000 K; the initial structure is

所有比例尺均为1.5 nm。

the same as that shown in **c**. All scale bars are 1.5 nm.

碳具有高升华温度约3900 K；其他元素，如铝或硅，在低于3000 K的温度下挥发。

high sublimation temperature of ~3,900 K; other elements such as

空气中的热重分析表明，FG产品的氧化稳定性高于其衍生原料(补充图15)，并且比使用

aluminium or silicon volatilize out at <3,000 K.

Hummers方法获得的还原氧化石墨烯更稳定。

Thermogravimetric analysis in air shows that FG products are more

oxidatively stable than the materials from which they are derived (Sup-

plementary Fig. 15) and more stable than reduced graphene oxide

在某些情况下，检测到氧化能残留物，这些残留物

obtained with Hummer's method[23]. In some cases, silicon oxide residues

来自多次使用后磨损的石英管。

are detected, which come from worn out quartz tubes after multiples

uses.

先前的研究表明，石墨烯可以在极高的温度下无需催化剂合成。

Previous studies have shown that graphene can be synthesized

然而，当如图所示优化

without catalysts at extremely high temperatures[24–26]. However, when

FG时，当控制反应时间和温度时，它可以具有非常高的质量。

FG is optimized as shown here, it can have exceptionally high quality

此外，电流可以促进

when the reaction time and temperature are controlled. Furthermore,

石墨烯的结晶。在FJH过程中，氢、氮和氧的脱气可能有助于在咖啡衍生FG中形成大而薄的石墨烯

the electric current can facilitate the crystallization of graphene[27].

片，因为这可能阻止石墨烯层的堆叠，从而允许片层进一步生长。

Degassing of hydrogen, nitrogen and oxygen during the FJH process

might contribute to the formation of large and thin graphene sheets

in coffee-derived FG because it could prevent stacking of graphene

layers, thereby permitting further growth[25,28,29].

为了评估FG快速生长的机制，我们采用了在LAMMPS包(见方法)中实现的具有AIREBO原

To assess the mechanism of the rapid FG growth, we employ large-

子间势的大规模模拟。

scale simulations with the AIREBO[30,31] interatomic potential as imple-

一些获得的结构如图3a-d所示。

mented in the LAMMPS package (see Methods)[32]. Some of the acquired

低密度材料在退火过程中产生海绵状结构(图3a)，

structures are shown in Fig. 3a–d. The low-density materials yield a

而密度的增加导致深度石墨化(图3c)。

sponge-like structure (Fig. 3a) during annealing, whereas increased

我们注意到低密度

density leads to a high level of graphitization (Fig. 3c). We note the

CB样品中石墨化程度较高，局部密度大幅增加，同时大孔隙率较高(图3d)。

high level of graphitization in the low-density CB sample, where the

substantially increased local density is combined with high macro-

此外，在模拟期间，通过sp2/sp3比率可以定量化退火过程(图3e，f)。

porosity (Fig. 3d). Additionally, the annealing process is quantified

我们发现，石墨烯的形成过程

by the sp^2/sp^3 ratio during simulation (Fig. 3e, f). We find that the gra-

在较低温度(<2000 K)下受到严重破坏，但在较高温度(5000 K)下会大大加速(图3g)，

phene formation process is strongly impaired at lower temperatures

这一趋势在实验上也证明了(图2f)。

(<2,000 K) but greatly accelerated at higher temperature (5,000 K)

对于炭黑，

(Fig. 3g)—a trend that is also suggested by experiments (Fig. 2f). In the

FJH过程中的连续缺陷修复导致最初大致呈球形的质心颗粒逐渐转变为多面体形状(图3d)，

case of carbon black, continuous defect healing during FJH results in

在TEM图像中以清晰定义的角度显示为条纹(见图1b、e)，进一步证实了所生产材料的低缺陷性质。

the gradual conversion of initially roughly spherical centroid particles

into polyhedral shapes (Fig. 3d) that appear as fringes at clearly defined

angles in TEM images (see Fig. 1 b, e), further confirming the low-defect

nature of the produced materials.

通过增加石英管的尺寸，FJH工艺得以放大。

The FJH process was scaled up by increasing the quartz tube size. With

使用直径为4mm、8mm和15mm的石英管，每批可分别合成30mg、120mg和1g FG。

quartz tubes of 4 mm, 8 mm and 15 mm diameter, 30 mg, 120 mg and 1 g

图4a显示了使用三种管径获得

of FG can be synthesized per batch, respectively. Figure 4a shows the

的CB-FG量。闪蒸越短管子越细，FG

amount of CB-FG obtained with the three tube sizes. The shorter flash

的I2D/G越高。为了在保持FG质量的同

from the smaller tube results in FG with a higher $I_{2D/G}$. To increase the

时增加反应量，使用扁管很有帮助，因为它们可以实现更高的冷却速率(图4a)。

batch size while maintaining FG quality, flat tubes are helpful because

对于工业生产，我们

they enable a higher cooling rate (Fig. 4a). For industrial production, we

设想该过程可以自动进行连续FG合成(补充图16)。

envision that the process can be automated for continuous FG synthesis

(Supplementary Fig. 16).

发现FG可分散在水/表面活性剂(Pluronic F-127)中，以提供高浓度的分散液，达到4 g/l

FG was found to be dispersible in water/surfactant (Pluronic F-127)

(图4b，补充图17)。

to give highly concentrated dispersions reaching 4 g l^{-1} (Fig. 4b, Sup-

使用有机溶剂时，FG具有高度的分散性(图4c)，这可归因于

plementary Fig. 17). Using organic solvents, FG has a high degree of

涡轮层状结构允许高效的剥离；层间引力远低于通过石墨剥离获得的常规排列的AB堆叠石墨烯。

dispersibility (Fig. 4c)[33–35], which can be attributed to the turbostratic

arrangement permitting efficient exfoliation; the interlayer attraction

forces are much lower than in conventionally arranged AB-stacked

graphene obtained by graphite exfoliation.

对FG复合材料进行了研究，发现在添加少量FG下，物理性能显著增强。

FG composites were explored, revealing considerably enhanced

含0.05%FG并固化28天的CB-FG水泥复合材

physical properties at small FG loadings. CB-FG–cement composites

料的抗压强度比不含FG的对照样品高约25%(补充图18)。

with 0.05% FG and cured for 28 days had ~25% higher compressive

strength than the FG-free control sample (Supplementary Fig. 18).

这种抗压强度的增强比最近报道的采用电化学剥离石墨烯增强的水泥复合材料的抗压强度值高出三倍，

This enhancement in the compressive strength is three times higher

石墨烯负载量相同，且略大于其他水泥-石墨烯复合材料的抗压强度。

than the values reported recently for cement composites reinforced

by electrochemically exfoliated graphene with the same graphene

loading, and slightly larger than those of other cement–graphene

FG含量为0.1%的CB-FG水泥复合材料的七天抗压强度和抗拉强度分别比无FG对

composites[36,37]. The seven-day compressive and tensile strength of

照样品高约35%和约19%(图4d)。

CB-FG–cement composites with 0.1% FG loading are ~35% and ~19%

higher, respectively, than those of the FG-free control sample (Fig. 4d).

这些增强几乎是其他报道的石墨烯水泥复合材料在相同添加量下的三倍，表明强度提高很快。

These enhancements are almost three times larger than those of

other reported graphene–cement composites with the same load-

CB-FG水泥复合材料的扫描电

ing, demonstrating rapid strength development. Scanning electron

子显微镜图像(补充图19)显示FG在水泥浆中均匀分布。

microscopy images of CB-FG–cement composites (Supplementary

Fig. 19) show a homogeneous distribution of FG in the cement matrix.

CB-FG水泥复合材料的性能大幅度提高，强度快速提高，这再次归因于涡轮层状CB-FG的高分散性，这

The largely enhanced properties and rapid strength development of

可用于更均匀和更坚固的复合材料(有关进一步解释，请参阅补充信息)。

CB-FG–cement composites is again attributed to the high dispers-

ibility of the turbostratic CB-FG, which results in greater homogeneity

and robust composites (see Supplementary Information for further

explanations).

此外，CB-FG有效地提高了聚合物的性能。

In addition, CB-FG effectively enhances polymer properties. A

与不含石墨烯的聚二甲基硅氧烷(PDMS)相比，0.1 wt%CB-FG聚二甲基硅氧烷(PDMS)复合材料

0.1 wt% CB-FG–polydimethylsiloxane (PDMS) composite showed ~250%

的抗压强度增加约250%(补充图20)。

increase in compressive strength compared with PDMS without gra-

phene (Supplementary Fig. 20).

为了证明其在电化学储能装置中的应用，C-FG和CPC-FG也被用作锂离子电容器和锂离子电池中

To demonstrate its applicability in electrochemical energy storage

的电极材料(补充图21)，证明了FG在新能源应用中的潜力。

devices, C-FG and CPC- FG were also used as electrode materials in a

Li-ion capacitor and a Li-ion battery (Supplementary Fig. 21), dem-

onstrating the potential to use FG in advanced energy applications.

综上所述，从超低成本碳源(如煤炭和石油焦)、可再生资源(如生物炭和橡胶轮胎)和混

In summary, a low-energy bottom-up synthesis of easily exfoliated tur-

合废物(包括塑料瓶和丢弃的食物)证明了一种低能耗且下而上合成易剥离涡轮层状石墨烯的方法

bostratic graphene was demonstrated from ultralow-cost carbon sources

(such as coal and petroleum coke), renewable resources (such as biochar

and rubber tyres) and mixed-waste products (including plastic bottles

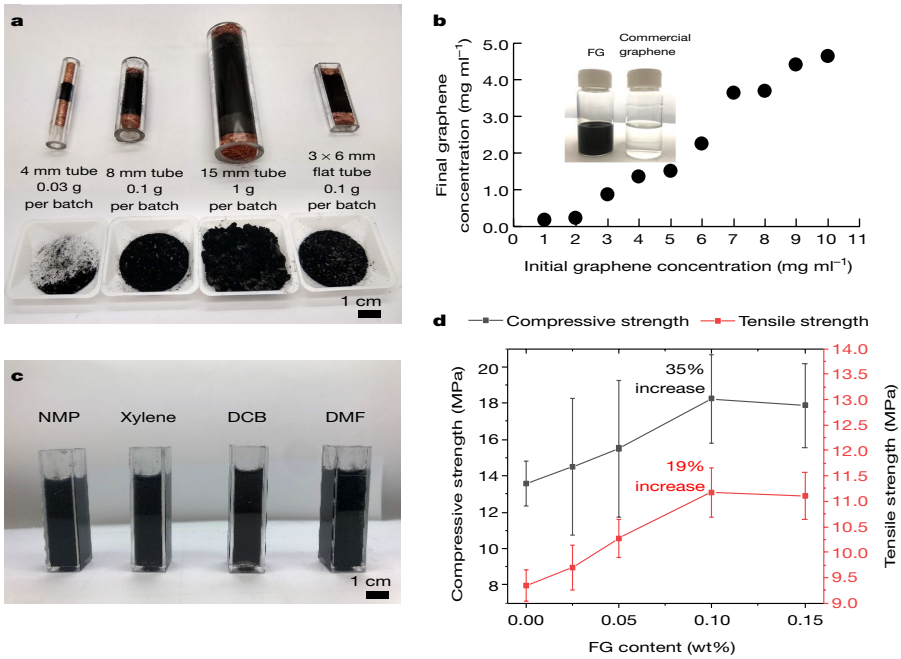

图4. CB-FG的放大和应用。 a. 不同材质的玛瑙石英管尺寸和形状，用于合成FG。 在每个试管中进行两个单独的合成过程，提供试管中的样品和塑料皿中的样品。 b. FG在水Pluronic(F-127)溶液(1%)中的分散。 照片显示了4 g/l CB-FG和10 g/l的上清液 离心后的商业样品。 在该浓度下，商用石墨烯作为胶体不稳定，导致离心后上清液中出现透明液体。 c. FG在各种有机溶剂中的分散度为5 g/l。 d. FG复合水泥的力学性能。 误差条表示一个标准误差(n=3)。

Fig. 4 | Scaling up and applications of CB-FG. a, FJH quartz tubes of different sizes and shapes, used to synthesize FG. Two separate synthesis processes were conducted with each tube, providing the samples in the tube and those in the plastic dishes. **b**, FG dispersion in a water–Pluronic (F-127) solution (1%). The photograph shows the supernatants of 4 g l^{-1} of CB-FG and of 10 g l^{-1} of a commercial sample after centrifugation. The commercial graphene was not stable as a colloid at this concentration, resulting in a clear liquid in the supernatant after centrifugation. **c**, FG dispersion in various organic solvents at 5 g l^{-1}. **d**, Mechanical performance of cement compounded with FG. The error bars represent one standard error ($n = 3$).

FG合成工艺的放大可以为块体结构复合材料提供涡轮层状石墨烯。

and discarded food). Scaling up of the FG synthesis process could provide turbostratic graphene for bulk construction composite materials.

Online content

Any methods, additional references, Nature Research reporting summaries, source data, extended data, supplementary information, acknowledgements, peer review information; details of author contributions and competing interests; and statements of data and code availability are available at https://doi.org/10.1038/s41586-020-1938-0.

1. Allen, M. J., Tung, V. C. & Kaner, R. B. Honeycomb carbon: a review of graphene. *Chem. Rev*. **110**, 132–145 (2010).
2. Yi, M. & Shen, Z. A review on mechanical exfoliation for the scalable production of graphene. *J. Mater. Chem. A* **3**, 11700–11715 (2015).
3. Hernandez, Y. et al. High-yield production of graphene by liquid-phase exfoliation of graphite. *Nat. Nanotechnol*. **3**, 563–568 (2008).
4. Eda, G., Fanchini, G. & Chhowalla, M. Large-area ultrathin films of reduced graphene oxide as a transparent and flexible electronic material. *Nat. Nanotechnol*. **3**, 270–274 (2008).
5. Li, D. et al. Processable aqueous dispersions of graphene nanosheets. *Nat. Nanotechnol*. **3**, 101–105 (2008).
6. Lin, L., Peng, H. & Liu, Z. Synthesis challenges for graphene industry. *Nat. Mater*. **18**, 520–524 (2019).
7. Ferrari, A. C. et al. Raman spectrum of graphene and graphene layers. *Phys. Rev. Lett*. **97**, 187401 (2006).
8. Ferrari, A. C. Raman spectroscopy of graphene and graphite: disorder, electron–phonon coupling, doping and nonadiabatic effects. *Solid State Commun*. **143**, 47–57 (2007).
9. Malard, L. M., Pimenta, M. A., Dresselhaus, G. & Dresselhaus, M. S. Raman spectroscopy in graphene. *Phys. Rep*. **473**, 51–87 (2009).
10. Ni, Z. H. et al. Probing charged impurities in suspended graphene using Raman spectroscopy. *ACS Nano* **3**, 569–574 (2009).
11. Garlow, J. A. et al. Large-area growth of turbostratic graphene on Ni (111) via physical vapor deposition. *Sci. Rep*. **6**, 19804 (2016).
12. Niilisk, A. et al. Raman characterization of stacking in multi-layer graphene grown on Ni. *Carbon* **98**, 658–665 (2016).
13. Li, Z. Q. et al. X-ray diffraction patterns of graphite and turbostratic carbon. *Carbon* **45**, 1686–1695 (2007).
14. Franklin, R. E. Crystallite growth in graphitizing and non-graphitizing carbons. *Proc. R. Soc. Lond*. **209**, 196–218 (1951).
15. Stankovich, S. et al. Synthesis of graphene-based nanosheets via chemical reduction of exfoliated graphite oxide. *Carbon* **45**, 1558–1565 (2007).
16. Cai, M., Thorpe, D., Adamson, D. H. & Schniepp, H. C. Methods of graphite exfoliation. *J. Mater. Chem*. **22**, 24992–25002 (2012).
17. Miandad, R. et al. Catalytic pyrolysis of plastic waste: moving toward pyrolysis based biorefineries. *Front. Energy Res*. **7**, 27 (2019).
18. Gibb, B. C. Plastics are forever. *Nat. Chem*. **11**, 394–395 (2019).
19. Parfitt, J., Barthel, M. & Macnaughton, S. Food waste within food supply chains: quantification and potential for change to 2050. *Philos. Trans. R. Soc. B* **365**, 3065–3081 (2010).
20. Gustavsson, J., Cederberg, C., Sonesson, U., van Otterdijk, R. & Meybeck, A. *Global Food Losses and Food Waste: Extent, Causes and Prevention* (FAO, 2011); http://www.fao.org/3/a-i2697e.pdf.
21. Jambeck, J. R. et al. Plastic waste inputs from land into the ocean. *Science* **347**, 768–771 (2015).
22. Yao, Y. et al. Carbothermal shock synthesis of high-entropy-alloy nanoparticles. *Science* **359**, 1489–1494 (2018).
23. Advincula, P. A. et al. Accommodating volume change and imparting thermal conductivity by encapsulation of phase change materials in carbon nanoparticles. *J. Mater. Chem. A* **6**, 2461–2467 (2018).
24. Chakrabarti, A. et al. Conversion of carbon dioxide to few-layer graphene. *J. Mater. Chem*. **21**, 9491–9493 (2011).
25. Lin, J. et al. Laser-induced porous graphene films from commercial polymers. *Nat. Commun*. **5**, 5714 (2014).
26. Nepal, A., Singh, G. P., Flanders, B. N. & Sorensen, C. M. One-step synthesis of graphene via catalyst-free gas-phase hydrocarbon detonation. *Nanotechnology* **24**, 245602 (2013).
27. Huang, J. Y. et al. Real-time observation of tubule formation from amorphous carbon nanowires under high-bias Joule heating. *Nano Lett*. **6**, 1699–1705 (2006).
28. Harris, P. J. F. Engineering carbon materials with electricity. *Carbon* **122**, 504–513 (2017).
29. Luong, D. X. et al. Laser-induced graphene fibers. *Carbon* **126** 472–479 (2017).
30. Stuart, S. J., Tutein, A. B. & Harrison, J. A. A reactive potential for hydrocarbons with intermolecular interactions. *J. Chem. Phys*. **112**, 6472–6486 (2000).
31. Brenner, D. W. et al. A second-generation reactive empirical bond order (REBO) potential energy expression for hydrocarbons. *J. Phys. Condens. Matter* **14**, 783–802 (2002).
32. Plimpton, S. Fast parallel algorithms for short-range molecular dynamics. *J. Comput. Phys*. **117**, 1–19 (1995).
33. Xu, Y. et al. Liquid-phase exfoliation of graphene: an overview on exfoliation media, techniques, and challenges. *Nanomaterials* **8**, 942 (2018).
34. O'Neill, A., Khan, U., Nirmalraj, P. N., Boland, J. & Coleman, J. N. Graphene dispersion and exfoliation in low boiling point solvents. *J. Phys. Chem. C* **115**, 5422–5428 (2011).
35. Dong, L. et al. A non-dispersion strategy for large-scale production of ultra-high concentration graphene slurries in water. *Nat. Commun*. **9**, 76 (2018).
36. Liu, J., Li, Q. & Xu, S. Reinforcing mechanism of graphene and graphene oxide sheets on cement-based materials. *J. Mater. Civ. Eng*. **31**, 04019014 (2019).
37. Krystek, M. et al. High-performance graphene-based cementitious composites. *Adv. Sci*. **6**, 1801195 (2019).

Article

Methods

FJH系统

FJH system

FJH设置详见补充图1。在石英管内，两个松散配合的

The FJH set up is detailed in Supplementary Fig. 1. Inside a quartz tube,

电极使用两个铜棉塞或石墨垫片压缩碳源，以接触碳源，从而允许释发性物质脱气。

two loosely fitting electrodes compress the carbon source using two

copper-wool plugs or graphite spacers to contact the carbon sources

压缩力可通过改进的小虎钳控制，以将

to allow degassing of volatile materials. The compressing force is

样品电阻降至1-1000Ω，并且是获得良好闪蒸反应(0.004-4 S/cm)的关键。

controllable by a modified small vice so as to minimize the sample

resistance to 1–1,000 Ω, and is key to obtaining a good flash reaction

为了控制放电时间，使用了具有可编程毫秒级延迟时间的机械继电器。

(0.004–4 S cm^{-1}). To control the discharge time, a mechanical relay with

整个样品反应管置于低压

programmable millisecond-level delay time is used. The entire sample

容器(塑料真空干燥器)内，以确保安全并便于脱气。

reaction chamber is placed inside a low-pressure container (plastic

然而，FJH工艺在

vacuum desiccator) for safety and to facilitate degassing. However, the

1个大气压下同样可以进行。电容器组由20个电容器组成，总电容为

FJH process works equally well at 1 atm. The capacitor bank consists

0.22 F。每个电容器通过断路器连

of 20 capacitors with a total capacitance of 0.22 F. Each capacitor is

接到主电源电缆(或母线)，断路器也用作开关，以启用/禁用每个电容器。

connected to the main power cable (or bus) by a circuit breaker that is

电容器组由一个400 V的电源

also used as a switch to enable/disable each capacitor. The capacitor

进行直流充电。第一个原型系

bank is charged by a d.c. supply capable of reaching 400 V. The first

统方便地放置在一个塑料移动车上(补充图1b)。

prototype system is placed conveniently on one plastic mobile cart

使用直径为15 mm的大石英管，我们使用FJH工艺每批

(Supplementary Fig. 1b). Using a large 15-mm-diameter quartz tube,

合成1 g FG。

we achieve synthesis of 1 g of FG per batch using the FJH process.

安全提示：电容器组能够产生致命的电脉冲。

Safety notice: the capacitor bank is capable of generating fatal elec-

因此，采取以下步骤保护操作员和电路，我们强烈建议遵循这些措施。

tric pulses. Therefore, the following steps are taken to protect the oper-

电路的详细信息可在补充图1a中找到。

ator as well as the circuit, and we strongly suggest that these measures

be followed. Details of the circuit can be found in Supplementary Fig. 1a.

在放电闪蒸过程中，应佩戴深色安全眼镜，以保护眼睛免受强光照射。

Darkened safety glasses should be worn to protect eyes from the bright

light during the discharge flashing process.

断路器的电压和电流额定值适用于每个电容器在50-200 ms放电时间的基础上向FJH放电提供的最

The voltage and current ratings for the circuit breaker are appropriate

大电压和预期最大电流。

for the maximum voltage and the anticipated maximum current that

will be supplied by each capacitor to the FJH discharge on the basis of

我们使用约400 V的最大充电和放电电压，最大电流

a discharge time of 50–200 ms. We use the maximum charging and

分别为0.7 A和0.1 A。

bleeding voltages at ~400 V with maximum currents of 0.7 A and 0.1 A,

样品的脉冲放电电压约为400 V，在<100 ms内，电流可达1000 A。

respectively. The pulse discharging voltage to the sample is ~400 V and

使用机械继电器时，使用24 mH电感

current can reach up to 1,000 A in <100 ms. A 24-mH inductor is used

器避免电流尖峰。如果没有电感器，

to avoid current spikes while using the mechanical relay. Without the

机械继电器在电路间歇闭合期间可能容易产生大电流电弧。

inductor, the mechanical relay could be prone to high-current arcing

为了在切断电流时保护电感器免受

during the intermittent closing of the circuit. To protect the inductor

尖峰电压的影响，将具有适当额定值的二极管和低电阻电阻并联到电感器上。

from the spike voltage when shutting off the current, a diode and a low-

resistance resistor with appropriate ratings are connected parallel to

此外，为了防止电容器在振荡衰减(可能发生在快速放电中)的情况下发生反

the inductor. Additionally, to protect the capacitor from reverse polar-

极性，将适当的二极管平行安装在电容器组上。

ity in case of oscillatory decay (which can occur in a fast discharge), an

appropriate diode is placed parallel to the capacitor bank.

表征

Characterization

使用FEI Helios NanoLab 660双光束SEM系统，在5 kV、工作距离为10 mm的条件下，通过扫描

The resultant FG products were characterized by scanning electron

电子显微镜(SEM)对生成的FG产品进行了表征。

microscopy (SEM) using an FEI Helios NanoLab 660 DualBeam SEM

使用PHI-Quantera SXM扫描

system at 5 kV with a working distance of 10 mm. X-ray photoelectron

X射线微探针，在5×10-9托的基础压力下收集X射线光电子能谱(XPS)数据。

spectroscopy (XPS) data were collected with a PHI Quantera SXM

Scanning X-ray Microprobe with a base pressure of 5×10^{-9} torr. Sur-

使用0.5-eV步长记录测量光谱，通过能量为

vey spectra were recorded using 0.5-eV steps with a pass energy of

使用0.1-eV步长记录元素光谱，通过能量为26 eV。

140 eV. Elemental spectra were recorded using 0.1-eV steps with a pass

以C 1s峰(284.5 eV)为参考，对所有XPS光谱进行了校正。

energy of 26 eV. All of the XPS spectra were corrected using the C 1*s*

peak (284.5 eV) as reference.

使用JEOL 2100F场发射枪在200 kV下拍摄TEM图像。

TEM images were taken with a JEOL 2100F field-emission gun TEM at

原子分辨率HR-TEM图像是在80千电子伏的FEI Titan Themis S/TEM系统上拍摄的。

200 kV. Atomic-resolution HR-TEM images were taken with an FEI Titan

通过将石墨烯样品(<200 μl)的稀释分散液

Themis S/TEM system at 80 keV. Samples were prepared by dropping

(约1 mg/ml的异丙醇溶液)滴在TEM-Cu网格上制备样品。

diluted dispersions (~1 mg ml^{-1} in isopropanol) of the graphene sample

使用浴式超声波仪(约15分钟)制备分散液。

(<200 μl) on the TEM Cu grids. The dispersion was prepared using a

电子衍射通过衍射标准(蒸发铝栅；Ted Pella)进行校准。

bath sonicator (~15 min). Electron diffraction was calibrated by a dif-

fraction standard (evaporated Al grid; Ted Pella).

在接触溶剂之前，使用Renishaw拉曼显微镜和功率为5 mW的532 nm激光，在玻片顶部用制备

All Raman spectra were collected with as-prepared FG samples atop a

好的FG样品收集所有拉曼光谱。

glass slide, before exposure to solvent, using a Renishaw Raman micro-

图1中的局部拉曼光谱使用50×

scope and a 532-nm laser with a power of 5 mW. A 50× lens was used

透镜，图2中的平均拉曼光谱使用5×透镜。

for the local Raman spectra in Fig. 1 and a 5× lens for the mean Raman

spectra in Fig. 2.

原子建模

Atomistic modelling

原子模拟是使用周期性边界条件进行的，除了包含约55000个原子的炭黑模型外，所有结构的每个单

Atomistic simulations were carried out using periodic bound-

元都有约15000个原子。

ary conditions with ~15,000 atoms per unit cell for all structures

except the carbon black model, which contained ~55,000 atoms.

初始构型是通过任意形状和直径达8-12的小石墨片的随机定位和错配定位，然后添加随机定位的

The initial configurations were created by random positioning and

单个碳原子(碳原子含量约为50%，以表示源材料的非石墨化部分)来创建的。

misorientation of small graphitic flakes of arbitrary shape and up to

8–12 Å in diameter, and subsequently adding randomly positioned

individual carbon atoms (the atomic carbon content was ~50% to

represent a non-graphitized portion of the source material). Car-

炭黑质心粒子是通过将随机取向的石墨薄片排列成大致球形，空心，直径达12 nm，并添加原子碳

bon black centroid particles were created by arranging randomly

(约50%)而形成的。

oriented graphitic flakes in roughly spherical shapes with hollow

cores and diameters of up to 12 nm, and adding atomic carbon

初始配置在400 K下进行2ns的初步退火，以消除结构创建规则引起的不合理性，

(~50%). The initial configurations were subjected to preliminary

然后使用温度阻尼参数为0.025×10 -12 s的Nose-Hoover恒温器(标准NVT系综)以0.5×10 -12 K/s

annealing at 400 K for 2×10^{-9} s to eliminate irregularities caused by

的加热速度加热到目标退火温度。

the structure creation protocol, then heated to the target annealing

temperature with a heating speed of 0.5×10^{-12} K s^{-1} using a Nose–

Hoover thermostat (canonical NVT ensemble) with a temperature

结构在目标退火温度下保持5×10 -9 s

damping parameter of 0.025×10^{-12} s. The structures were held

(炭黑为15×10 -9 s)。

at the target annealing temperatures for 5×10^{-9} s (15×10^{-9} s for

carbon black).

水溶液中闪蒸石墨烯分散液的制备

Preparation of flash graphene dispersion in water–Pluronic solution

将FG分散在浓度为1-10 g/l的水-Pluronic(F-127)溶液(1%)中。

FG was dispersed in water–Pluronic (F-127) solution (1%) at con-

将混合物在超声浴中超声处理40分钟，以获得深色分散液。

centrations of 1–10 g l^{-1}. The mixture was sonicated in an ultrasonic

使用配有19 cm半径转子的

bath for 40 min to obtain a dark dispersion. The dispersion was

Beckman Coulter Allegra X-12离心机，在1500 rpm(470相对离心力)下离心分散液30分钟，

subjected to centrifugation at 1,500 rpm (470 relative centrifugal

以去除大块材料。

force) for 30 min to remove aggregates using a Beckman Coulter

Allegra X-12 centrifuge equipped with a 19-cm-radius rotor. The

通过紫外-可见光谱(岛津)分析上清液。

supernatant was analysed via ultraviolet–visible spectroscopy

将分散液稀释500倍，并在660 nm处记录吸光度。

(Shimadzu). The dispersions were diluted 500 times and the

使用α 660=6600 l/g·m的消光系

absorbance was recorded at 660 nm. An extinction coefficient

数计算溶液中石墨烯的浓度。

of α_{660} = 6,600 l g^{-1} m^{-1} was used to calculate the concentration of

graphene in the solution.

水泥样品制备

Cement sample preparation

将不同浓度的FG分散在1%水Pluronic(F-127)溶液中。

FG at various concentrations was dispersed in 1% water–Pluronic (F-127)

使用剪切混合器(Silverson L5MA)在5000 rpm下搅拌分散液15分钟。

solution. The dispersion was agitated for 15 min at 5,000 rpm using a

将水中的石墨烯悬浮液与水灰比为0.40的硅酸盐水泥混合。

shear mixer (Silverson L5MA). The graphene suspension in water was

mixed with Portland cement with a water-to-cement ratio of 0.40. The

将浆料浇注在5×5×5 cm3立方体聚四氟乙烯模具(用于抗压强度测量)和2.5 cm×3.8 cm圆柱形模

slurry was cast in 5 × 5 × 5 cm^3 cubic polytetrafluoroethylene moulds (for

具(用于抗拉强度测量)中。

compressive strength measurements) and in 2.5 cm × 3.8 cm cylindrical

24小时后，将所有立方体和圆柱体

moulds (for tensile strength measurements). All cubes and cylinders

取出模具，并放置在水中再固化24小时。

were taken out the moulds after 24 h and placed in water for curing

在第7天和第28天后测量压缩和拉伸机械强度。

for another 24 h. The compressive and tensile mechanical strengths

对于每个FG水泥比例，浇筑并测试三个样品。

were measured after 7 and 28 days. For each FG–cement ratio, three

samples were cast and tested.

水泥和PDMS测试程序

Cement and PDMS testing procedures

抗压强度。压缩强度试验是使用Forney变频驱动自动机器进行的，该机器

Compressive strength. The compression strength tests were per-

具有双称重传感器，以达到最大精度。

formed using a Forney Variable Frequency Drive automatic machine

with dual load cells for maximum accuracy.

抗拉强度。由于水泥基材料的脆性，通过劈裂试验计算抗拉强度，因为它提供了最准

Tensile strength. Owing to the brittle nature of cement-based mate-

确的测量结果。

rials, the tensile strength was calculated via a splitting test because it

特殊夹具固定圆柱体，从而使施加在样品底

gives the most accurate measurement. Special jigs held the cylinders

面和顶面中心线上的单轴压缩力在接触点之间产生拉伸应力。

so that the uniaxial compressive force applied to the centre lines of the

bottom and top surfaces of the samples caused tensile stress between

the points of contact.

Data availability

The datasets generated and/or analysed during the current study are available from the corresponding author on reasonable request.

Acknowledgements We thank G. A. Lopez Silva for preparing the schematic of the FJH process, J. Li for preparing the olive oil soot, Oxbow Calcining International LLC for donating the calcined coke, Ergon Asphalt and Emulsions, Inc. for donating the rubber-tyre-derived carbon black, and Neroval LLC for donating the biochar. K.V.B. and B.I.Y. thank the National Science Foundation (NSF) for support (CBET-1605848) and B. Sastri of the US Department of Energy for discussions. R.S. thanks the partial support of NSF-DMR 1709051. J.M.T. thanks the US Air Force Office of Scientific Research (FA9550-19-1-0296) for support.

Author contributions D.X.L. discovered the FJH conversion of carbon materials to graphene, designed and built the FJH apparatus, designed and built the spectrometer for temperature determination, acquired most of the data, and wrote most of the manuscript. K.V.B. conducted the mechanistic theory calculations under the guidance of B.I.Y. W.A.A. and P.A.A. fabricated some FG samples, and blended and tested the polymer blends. M.G.S. obtained the SEM images and wrote parts of Supplementary Information, especially regarding FG morphology. C.K. assisted with the design of the FG apparatus and the spectrometer, and wrote parts of Supplementary Information regarding turbostratic graphene. R.V.S. obtained most of the TEM images and all of the selected-area electron diffraction data. W.C. and H.G. obtained some of the TEM images. M.R. built and tested the lithium-ion capacitor. C.K. and V.M. assisted D.X.L. in the design and safety features of the FJH system. E.A.M. performed the thermogravimetric analysis. Z.W. obtained the surface area. M.B. obtained the cement and polymer composite data under the guidance of R.S. All aspects of the research were overseen by J.M.T., who co-wrote some sections of the manuscript.

Competing interests The FG synthesis process is the intellectual property of Rice University. J.M.T., D.X.L. and V.M. will be stockholders in Universal Matter Ltd, a company licensing the FG intellectual property of Rice University and scaling up this process. At the time of the writing and submission of this manuscript, the license to Universal Matter has not been consummated. C-Crete Technologies owns intellectual property on the strengthening of graphene–cement/concrete composites. V.M. is now employed by Universal Matter. D.X.L. and J.M.T. will remain full time with Rice University, whereas D.X.L. might be employed by Universal Matter in two years. All conflicts of interest for J.M.T. and D.X.L. are managed through regular disclosure to the Rice University Office of Sponsored Programs and Research Compliance.

Additional information

Supplementary information is available for this paper at https://doi.org/10.1038/s41586-020-1938-0.

Correspondence and requests for materials should be addressed to R.S., B.I.Y. or J.M.T.

Peer review information *Nature* thanks Loh Kian Ping and the other, anonymous, reviewer(s) for their contribution to the peer review of this work.